Magnetic Surfaces and Localized Perturbations in the Wendelstein VII-A Stellarator

H. Wobig
Max-Planck-Institut für Plasmaphysik, EURATOM Association, D-8046 Garching, FRG

Z. Naturforsch. **42 a,** 1054–1066 (1987); received April 16, 1987

Dedicated to Professor Dieter Pfirsch on his 60th Birthday

The critical dependence of plasma confinement in low-shear stellarators, such as Wendelstein VII-A, on the external rotational transform can be explained on the basis of magnetic surface destruction. External symmetry-breaking perturbations generate islands on the low order rational magnetic surfaces. The islands are largest at $t = 1/2$ and $t = 1/3$. Confinement is optimum in close proximity to these values. In order to study the structure of surfaces under the influence of perturbations, a mapping procedure is used instead of field line integration. It is found that the neighbourhood of low-order rational surfaces is particularly robust against surface destruction. The reason is that in this vicinity only rational surfaces with large m and n exist ($t = m/n$). On these surfaces the external perturbation only generates small islands.

In W VII-A the current leads to the helical windings are one symmetry-breaking perturbation, and there might also be others. It is possible to avoid field errors of this kind in future stellarators.

I. Introduction

Experiments in low-shear stellarators like W VII-A [1] exhibit a critical dependence of the plasma confinement on the structure of the magnetic field. At particular values of the rotational transform t ($t = 1/2, 1/3, 2/5, \ldots$) confinement is deteriorated, which indicates that around these low-order rational values of t magnetic surfaces are destroyed by perturbation fields. The experimental results indicate that the perturbation breaks the five fold symmetry of the configuration and therefore can be explained by field errors coming from the coil system. Numerical calculations [2] have indeed shown that current leads to the helix create a local perturbation field of 10–20 G, which gives rise to island formation on rational surfaces. The largest islands occur at $t = 1/2$, three smaller islands at $t = 1/3$ and five islands at $t = 2/5$. Islands are also found at $t = 3/7$ and $t = 3/8$. It is not surprising to find enhanced plasma losses in the presence of such islands. As can be seen from Fig. 1 and 2 the energy content of the plasma is a minimum at $t = 1/2, 1/3, 2/5, 2/3, \ldots$.

What is surprising, however, is the maximum energy content in close proximity to $t = 1/2$ and $t = 1/3$. There is a small positive shear in W VII-A so that under these conditions the rotational transform ranges from $t = 0.48$ on the magnetic axis to $t = 0.49$ on the plasma boundary. A similar situation is $t = 0.51$ on the axis and 0.52 on the boundary. As already shown by numerical calculations the surfaces close to $t = 1/2$ or $t = 1/3$ are not destroyed by the perturbation which creates large islands at $t = 1/2$ or $1/3$. This can be understood from the distribution of rational numbers in the vicinity of $t = 1/2$ or $1/3$. Close to $1/2$ only rational numbers m/n exist with relatively high values of m and n. The distribution of rational numbers is shown in Fig. 3, where $|\log 1/n|$ is plotted vs $t = m/n$*. An t-interval from $t = 0.48$ to 0.49 contains rational surfaces with larger values of m and n than the region from $t = 0.44$ to $t = 0.45$. A magnetic field perturbation $\mathbf{B}_1$, which is created internally or externally, contains several Fourier harmonics, which are in resonance at $t = m/n$ and create a chain of at least n islands. With a decreasing perturbation spectrum, we expect the size of islands to decrease strongly with the period n (n is the number

Reprint requests to Dr. H. Wobig, Max-Planck-Institut für Plasmaphysik, D-8046 Garching.

* This figure has been prepared by I. and W. Ott.

0932-0784 / 87 / 1000-1054 $ 01.30/0. – Please order a reprint rather than making your own copy.

Dieses Werk wurde im Jahr 2013 vom Verlag Zeitschrift für Naturforschung in Zusammenarbeit mit der Max-Planck-Gesellschaft zur Förderung der Wissenschaften e.V. digitalisiert und unter folgender Lizenz veröffentlicht: Creative Commons Namensnennung-Keine Bearbeitung 3.0 Deutschland Lizenz.

This work has been digitalized and published in 2013 by Verlag Zeitschrift für Naturforschung in cooperation with the Max Planck Society for the Advancement of Science under a Creative Commons Attribution-NoDerivs 3.0 Germany License.

Zum 01.01.2015 ist eine Anpassung der Lizenzbedingungen (Entfall der Creative Commons Lizenzbedingung „Keine Bearbeitung") beabsichtigt, um eine Nachnutzung auch im Rahmen zukünftiger wissenschaftlicher Nutzungsformen zu ermöglichen.

On 01.01.2015 it is planned to change the License Conditions (the removal of the Creative Commons License condition "no derivative works"). This is to allow reuse in the area of future scientific usage.

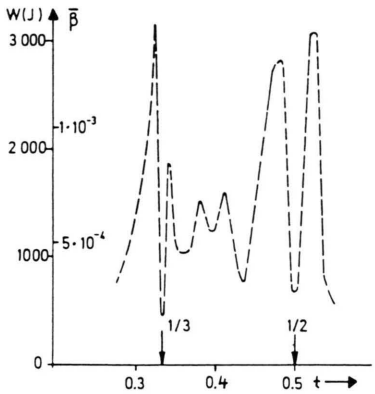

Fig. 1. Total plasma energy in W VII-A as a function of the external rotational transform t_0. Heating by neutral beam injection. W7A; D_2; NI; H_2; $\mathbf{B}_0 = 3-3.1$ T.

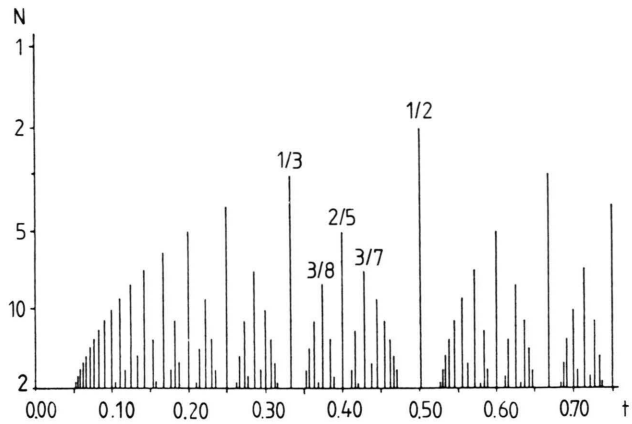

Fig. 3. Fractal diagram of rational numbers. The vertical axis is $|\log 1/n|$, the horizontal axis is m/n.

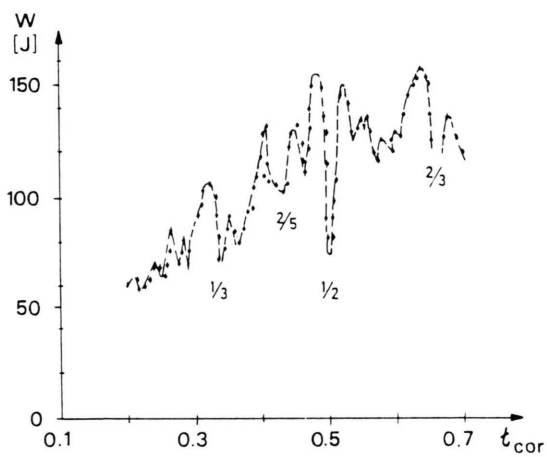

Fig. 2. Energy content as a function of t_0. Electron cyclotron heating. W7A; ECRH; 28 GHz; TE11; # 44621–44698; $P_N \sim 150$ kW; $\langle n \rangle \sim 5 \cdot 10^{12}$ cm^{-3}.

of toroidal transits before the magnetic island closes upon itself). This general behaviour may explain why the neighbourhood of low-order rational surfaces is especially robust against destruction.

The perturbations from the helix leads and joints are the only ones to be identified in the W VII-A device. Other unknown error fields could also be present in the coil arrangement or originate from ferromagnetic or paramagnetic material. The particular role of $t = 1/2$ and $t = 1/3$ can only be explained by a symmetry-breaking external perturbation, otherwise $t = 5/n$ should be the surfaces to be destroyed first. The basic periodicity of the W VII-A stellarator is $m = 5$.

The main question now is whether the neighbourhood of low-order rational surfaces is always the last one to be destroyed by any external or internal perturbation. In order to study the structure of perturbed magnetic surfaces, field line tracing would be the appropriate method, however, but great numerical effort is required. The mapping technique developed by Greene [3]–[4] and Chirikov [5] needs much less computer time. The disadvantage is that in general the analytic representation of the map corresponding to a perturbation field $\mathbf{B}_1(x)$ is not known, approximations have to be found. But it is well-known that any toroidal magnetic field with field lines returning to the poloidal plane after a toroidal transit provides a flux-conserving map of the poloidal plane onto itself. Studying the features of a flux (or area) conserving two-dimensional map is therefore equivalent to investigating toroidal flux surfaces with small perturbations. The theory of flux-conserving maps is well established. The KAM theorem states that irrational magnetic surfaces remain unperturbed if the perturbation is small enough [6]. Most theories of flux-conserving maps concentrate on the transition to chaos and the intrinsic scaling laws. In this context the question will be treated how configurations with different t-regime react on a fixed perturbation.

II. Basic Equations

We start from a magnetic field $\mathbf{B}_0$ and assume the existence of nested toroidal magnetic surfaces $\psi = \text{const}$. The field may be a vacuum field or a finite-β equilibrium field. Let the unperturbed magnetic field $\mathbf{B}_0$ be represented in flux coordinates (ψ, θ, φ) with the toroidal and poloidal coordinates φ and θ:

$$\mathbf{B}_0 = \nabla\psi \times \nabla(t\,\varphi - \theta)\,. \tag{1}$$

The rotational transform $t(\psi) = t_0 + t_1\,\psi + t_2\,\psi^2$ is specified by three constants t_0, t_1, t_2. In the poloidal plane with (ψ, θ) coordinates the twist map T_0

$$\psi_1 = \psi_0\,; \quad \theta_1 = \theta_0 + 2\,\pi\,t(\psi_1) \tag{2}$$

yields the Poincaré plot of the unperturbed surfaces. The unperturbed surfaces are circles in this coordinate system. The perturbation field $\mathbf{B}_1$ leads to a perturbed map $T_0 + T_1$ which can be derived from a generating function

$$S(\psi_1, \theta_0) = \psi_1\,\theta_0 + 2\,\pi \int^{\psi_1} t(\psi)\,\mathrm{d}\,\psi + h(\psi_1, \theta_0) \tag{3}$$

by

$$\psi_0 = \frac{\partial S}{\partial \theta_0}\,; \quad \theta_1 = \frac{\partial S}{\partial \psi_1}\,. \tag{4}$$

Owing to this procedure the determinant of the transformation is unity and the magnetic flux is automatically conserved. The function $h(\psi_1, \theta_0)$ represents the effect of the perturbation field $\mathbf{B}_1$. In general the relation between $\mathbf{B}_1$ and $h(\psi_1, \theta_0)$ is unknown, except in the case of a perturbation localized in the toroidal angle φ. With such δ-like dependence the field line equations can be integrated explicitly to yield the action-generating function $h(\psi_1, \theta_0)$.

In order to study the effect of perturbations in the W VII-A stellarator, the following ansatz for $h(\psi_1, \theta_0)$ is made: $h = \psi_1\,g(\theta_0)$ where g is a Fourier series in $\sin l\,\theta_0$ ($l = 1, 2, \ldots, 15$). This map roughly corresponds to an external error field which decreases towards the magnetic axis. The Fourier coefficients of $g(\theta_0)$: $K_1, \ldots, K_{15}$ are the control parameters of the map. The radial dependence of the generating function is somewhat arbitrary, it mainly describes the fact that the perturbation decreases towards the magnetic axis and leaves the magnetic axis invariant. The number of Fourier harmonics in $g(\theta_0)$ is limited to 15. This seems to be sufficient to describe a poloidal localized perturbation. In principle every Fourier harmonics separately depends on the flux coordinate, in that case the analytical representation of the map becomes rather complicated. It will be shown later on that the local properties of the map can be studied without the knowledge of the detailed radial dependence of the Fourier harmonics. With this model the following questions can be studied:

How are magnetic surfaces destroyed by increasing the control parameters?

What regime in t is most resistant to destruction?

III. Localized Perturbations

In general the relation between the perturbed map $T_0 + T_1$ can only be obtained by integrating the field line equations explicitly. In the case of a perturbation localized in the toroidal direction this integration can be reduced to one or a few steps. In order to investigate this situation, we start from the Hamiltonian form of the field line equations, which has been pointed out by many authors [7], [8], [9]. If (ψ, θ, φ) is the natural coordinate system of the unperturbed magnetic field $\mathbf{B}_0$ the magnetic field line equations in this coordinate system are

$$\frac{\mathrm{d}\psi}{\mathrm{d}\varphi} = \frac{B^\psi}{B^\varphi}\,, \quad \frac{\mathrm{d}\theta}{\mathrm{d}\varphi} = \frac{B^\theta}{B^\varphi}\,. \tag{5}$$

With the vector potential $\mathbf{A} = (0, A_\theta, A_\varphi)$ the magnetic field is given by

$$B^\psi = 1/\sqrt{g}\left(\frac{\partial A_\varphi}{\partial \theta} - \frac{\partial A_\varphi}{\partial \varphi}\right),$$

$$B^\theta = -\,1/\sqrt{g}\,\frac{\partial A_\theta}{\partial \psi}\,,$$

$$B^\varphi = 1/\sqrt{g}\,\frac{\partial A_\theta}{\partial \psi}\,. \tag{6}$$

$g^{i,k}$ is the metric tensor of the ψ, θ, φ coordinate system and $\sqrt{g}\,\mathrm{d}\psi\,\mathrm{d}\theta\,\mathrm{d}\varphi$ the volume element. By making the following identifications $H = A_\varphi$, $p = -A_\theta$ the field line equations can be written in canonical form [7]:

$$\frac{\mathrm{d}p}{\mathrm{d}\varphi} = -\frac{\partial H}{\partial \theta}\,, \quad \frac{\mathrm{d}\theta}{\mathrm{d}\varphi} = \frac{\partial H}{\partial p}\,. \tag{7}$$

p, θ are the canonical variables. The solution of these equations can be considered as a sequence of successive canonical transformations which map the point $P_k = (p_k, \theta_k)$ onto the successor $P_{k+1} = (p_{k+1}, \theta_{k+1})$ by

$$p_{k+1} = p_k - \frac{\partial}{\partial \theta_k} \{H(\theta_k, p_{k+1}, \varphi_k)\, \delta\varphi\},$$

$$\theta_{k+1} = \theta_k + \frac{\partial}{\partial p_{k+1}} \{H(\theta_k, p_{k+1}, \varphi_k)\, \delta\varphi\}. \quad (8)$$

$\delta\varphi$ is the step size along the field line. The advantage of this procedure is that each step is area-preserving (the functional determinant of the transformation $P_k \to P_{k+1}$ is unity). This property is also maintained in the case of approximations. The question now is how to relate the generating function $H\,\delta\varphi$ to the perturbation field $\mathbf{B}_1$.

In the unperturbed case the vector potential of the magnetic field is

$$\mathbf{A}_0 = -\psi \nabla\theta + \int^{\psi} t(\psi)\, \mathrm{d}\psi \nabla\varphi. \quad (9)$$

In the unperturbed region the Hamiltonian H_0 and the momentum variable p are therefore

$$H_0 = \int^{\psi} t(\psi)\, \mathrm{d}\psi, \quad p = \psi. \quad (10)$$

Owing to the perturbation field $\mathbf{B}_1$ additional terms appear:

$$H = H_0(\psi) + A^1_\varphi(\psi, \theta, \varphi), \quad p = \psi + A^1_\theta(\psi, \theta, \varphi). \quad (11)$$

In this case ψ and θ are no longer canonical variables, in the Hamiltonian $H(\psi, \theta, \varphi)$ the variable ψ has to be replaced by p. If the toroidal component of the magnetic field B^φ does not vanish the second equation in (10) can always be solved for ψ and we may write

$$\psi = p - A^1_\theta(\psi(p), \theta, \varphi). \quad (12)$$

The resulting Hamiltonian is

$$H(p, \theta, \varphi) = H_0(p - A^1_\theta(p, \theta, \varphi)) + A^1_\varphi(p, \theta, \varphi), \quad (13)$$

or by taking only the lowest order terms in the perturbation

$$H(p, \theta, \varphi) = H_0(p) + A^1_\varphi - t(p) A^1_\theta =: H_0 + H_1. \quad (14)$$

The Hamiltonian (14) describes the exact orbits of the field lines and one could reveal the structure of the surfaces by straightforward integration of the canonical equations. Field line equations in Hamiltonian formalism have attracted quite a number of theoreticians in the past, recently Elsässer [10] has applied this formalism to magnetic surface destruction in tokamaks and he derived critical perturbations from Chirikov's overlap criterion. Application of this criterion to W VII-A may already explain a general feature of this configuration. In order to demonstrate this let us assume the perturbation field given in a Fourier series in φ and θ. The perturbed Hamiltonian can be written

$$H_1 = \sum \varepsilon_{l,m}\, e^{i(l\theta + m\varphi)} \quad (15)$$

with the Fourier coefficients $\varepsilon_{l,m}$ converging to zero for $l, m \to \infty$. All Fourier harmonics generate islands on rational magnetic surfaces with $t(p) = m/l$. The size of these primary islands is

$$\Delta_{l,m} = 4\sqrt{\varepsilon_{l,m}/t'}$$

($\varepsilon_{l,m}$ and the shear t' haved to be taken at the resonant surface). This formula shows the well-known property of island reduction by increasing the shear. The conclusion would be that small shear stellarators are more vulnerable to fixed perturbations than high shear ones. Let us assume, however, that the Fourier spectrum is limited to a large but finite number of harmonics ($l \leqq L$, $m \leqq M$). Then there is a minimum distance of adjacent resonant surfaces on the t-scale:

$$\min \left| \frac{m}{l} - \frac{m'}{l'} \right| = d_0 > 0.$$

In such a case one could choose a shear small enough to avoid primary islands across the plasma radius. If we approximate t by $t = t_0 + t_1 p$ the variation of t across the radius is $\delta t = t_1 p_b$ (p_b is the boundary value of the flux coordinate). Now, if δt is chosen smaller than d_0, primary islands can be avoided. In practice, however, the shear is given and a certain number of islands have to be tolerated. In that case t_0 can be selected such as to make primary islands as small as possible. This is the case, if l and m – the mode numbers of the rational surfaces ar as large as possible, since the $\varepsilon_{l,m}$ are generally decreasing with increasing l and m, the size of the primary islands follows.

In order to select an appropriate t-regime with high order rational surfaces a well-known feature of

rational numbers is very useful. This states that in the very neighbourhood of rational numbers with low l and m ($t = 1/2$ or $1/3$) only high order rational numbers exist. Consider for instance the sequence $t_n = 1/(2 + 1/n)$ with $n \to \infty$. This sequence converges to $t = 1/2$ as is indicated in Figure 3. The corresponding sequence of rational surfaces converges towards the separatrix, which in general is stochastic. There exists a critical t-value close to the low order rational surface from where on the surfaces are destroyed. This prevents us to approach the low order rational surface too close. The best choice for t and t_1 is

$$t_n \leqq t_0 + t_1 p \leqq t_{n'} \leqq t_{\text{crit}} ,$$

and n, n' as large as possible. t_{crit} is the transform of the last rational surface before the stochastic layer.

A critical situation may arise if across the plasma radius two or more primary islands exist. Secondary islands appear with increasing amplitude $\varepsilon_{l,m}$ and the region between two adjacent primary islands becomes stochastic. The threshold for stochasticity is given by Chirikov's overlap criterion which states that this region exhibits stochasticity, if

$$\frac{1}{2} t' \Delta_{l,m} + \frac{1}{2} \Delta_{l',m'} \geqq \frac{2}{\pi} \left| \frac{m}{l} - \frac{m'}{l'} \right|$$

or

$$\sqrt{\varepsilon_{l,m} t'} + \sqrt{\varepsilon_{l',m'} t'} \geqq \frac{4}{\pi} \left| \frac{m}{l} - \frac{m'}{l'} \right| . \qquad (16)$$

A first conclusion from this inequality is that small is helpful in preventing the stochastic instability. The threshold for stochasticity depends on the product $\varepsilon_{l,m} t'$, therefore a high shear system will be more easily destroyed than a low shear system.

The conclusions drawn so far are quite general without referring to the specific nature of the perturbation. To proceed further we consider a similar situation as it is found in the periodically kicked pendulum where the driving force is a delta-function in time. Owing to our assumption of a localized perturbation the function H_1 vanishes everywhere except in a small neighbourhood of $\varphi = \varphi_s$. Let $\delta\varphi$ be the length of this interval. In this region the main contribution to a displacement of the field line comes from the perturbation, and the transformation of the coordinates p, θ across this region is given by

$$p_2 = p_1 - \frac{\partial}{\partial \theta_1} \{H_1 (p_2, \theta_1, \varphi_s)\, \delta\varphi\} ,$$

$$\theta_2 = \theta_1 + \frac{\partial}{\partial p_2} \{H_1 (p_2, \theta_1, \varphi_s)\, \delta\varphi\} . \qquad (17)$$

The index 1 indicates a point at the beginning of the perturbed region and the index 2 a point at its end. When a field line is followed once around the torus, this displacement has to be added to the unperturbed orbit described by $H_0(p)$. Outside the perturbed interval the coordinates ψ, θ are canonical variables and to describe the final map it is justified to return to these variables.

From the preceding analysis it follows that the unknown perturbation $h(\psi_1, \theta_0)$ is given by $H_1(\psi_1, \theta_o, \varphi_s)\, \delta\varphi$. Here the index o indicates a point in the poloidal plane $\varphi = 0$ and the index 1 its image after one toroidal transit. If we write the map T in the coordinates of the unperturbed field only the t-profile is left to describe the different unperturbed cases. The detailed geometry, however, enters into the perturbed map $T_0 + T_1$ since the function H_1 depends on the covariant components of the vector potential $\mathbf{A}_1$. The metric tensor of the coordinate system (ψ, θ, φ) therefore appears in H_1.

In order to obtain a rough estimate of the function h, we consider the special case with $A_\theta = 0$: the perturbation field only consists of a θ-component and a ψ-component, the φ-component being zero. This is no loss of generality, since the φ-component does not lead to displacement of the field line. The φ-component of $\boldsymbol{A}_1$ is found from

$$A_\varphi = \int \sqrt{g}\, B^\psi \, \mathrm{d}\theta$$

with $B^\psi = \vec{B}_1 \cdot \nabla\psi =: B_{1,n} |\nabla\psi|$. $B_{1,n}$ is the component of the perturbation field in the normal direction to the unperturbed magnetic surface. Neglecting the θ-dependence of g and $|\nabla\psi|$, we can approximate A_φ by

$$A_\varphi = B_0\, \varepsilon \sqrt{g}\, |\nabla\psi| \int f(\psi, \theta)\, \mathrm{d}\theta .$$

Here B_0 is a measure of the toroidal field and ε is the amplitude of the perturbation field normalized to the total toroidal field B_0. The function $f(\theta)$ is of the order one and describes the poloidal variation of the perturbation field. The metric $\sqrt{g}$ and $|\nabla\psi|$ can be estimated from the volume of the magnetic

surface

$$V = 2\pi a^2 R = \int \sqrt{g}\, d\psi\, d\theta\, d\varphi .$$

R is the major radius of the magnetic surface and a the effective minor radius. As an approximation we obtain

$$\int \sqrt{g}\, d\psi\, d\theta\, d\varphi = 4\pi^2 \psi \sqrt{g} ,$$

and from this relation

$$\sqrt{g}\, |\nabla \psi| = R a = A a^2 .$$

Here A is the aspect ratio of the magnetic surface. In summary the perturbation function h is

$$h(\psi, \theta) = B_0 a^2 A\, \varepsilon f(\psi, \theta)\, \delta\varphi , \tag{18}$$

where f is a function of order one. The function ψ has the dimension of a magnetic flux. ψ can be made dimensionless by dividing by $B_0 a^2$.

Then the generating function $S(\psi, \theta)$ of the map T can be written

$$S(\psi_1, \theta_0) = \psi_1 \theta_0 + 2\pi \int^{\psi_1} t(\psi)\, d\psi + A\, \varepsilon f(\psi_1, \theta_0)\, \delta\varphi . \tag{19}$$

The map described by this generating function follows from (3). In order to obtain an explicit form, these equations have to be solved for ψ_1 and θ_1. To find an analytic solution, a linear ansatz in ψ_1 is made,

$$A\, \varepsilon\, \delta\varphi\, f(\psi_1, \theta_0) = h(\theta_0) + \psi_1 g(\theta_0) , \tag{20}$$

which yields

$$\psi_1 = \frac{\psi_0 - h'(\theta_0)}{1 + g'(\theta_0)} ,$$

$$\theta_1 = \theta_0 + 2\pi t(\psi_1) + g(\theta_0) . \tag{21}$$

In case of $g = 0$ this is the well-known twist map, which in its simplest version ($h' = K \sin\theta_0$, $t(\psi) = \psi$) is the standard map of Chirikov and Taylor.

In the special case $h = 0$ we obtain the map

$$\psi_1 = \frac{\psi_0}{1 + g'(\theta_0)} ,$$

$$\theta_1 = \theta_0 + 2\pi t(\psi_1) + g(\theta_0) . \tag{22}$$

These equations are the basis for the numerical calculations described in the following section. As an example we consider the WVII-A stellarator with an aspect ratio of $A = 20$. Let the maximum perturbation be 30 G and the region of localization $\delta\varphi = 1/20$ which corresponds to 60 cm on the circumferene. In this case the perturbation function $A\, \varepsilon f\, \delta\varphi$ is of the order 10^{-3}.

In general the generating function is nonlinear in ψ, but it can be shown that locally the map can be approximated by a twist map. For this purpose we expand the generating function around $\bar{\psi}$ and introduce a new variable $x = \psi - \bar{\psi}$ with

$$f = f(\bar{\psi}, \theta_0) + f'(\bar{\psi}, \theta_0)\, x + \ldots . \tag{23}$$

If we neglect quadratic or higher order terms in x the map reduces to that given by (20). Neglecting even the linear terms in x yields

$$x_1 = x_0 - \frac{\partial f}{\partial \theta_0} , \quad \theta_1 = \theta_0 + 2\pi t(\bar{\psi}) + 2\pi t'(\bar{\psi})\, x_1 . \tag{24}$$

This can be reduced to a standard twist map by defining a new variable y by $y = t(\bar{\psi}) + t'(\bar{\psi})\, x$. The resulting map is

$$y_1 = y_0 - t'(\bar{\psi}) \frac{\partial f}{\partial \theta_0} ,$$

$$\theta_1 = \theta_0 + 2\pi y_1 . \tag{25}$$

If the perturbation f contains only one harmonic $f = A \cos\theta$, this approximation yields the standard Chirikov Taylor map with the control parameter $K = 2\pi t' A$. As is known from the theory of the standard map, there are no *KAM*-surfaces above $K = 1$. Since the control parameter is proportional to the shear t', this result says that high shear systems exhibit stochastic instability at a smaller perturbation level than low shear configurations. Since t' occurs as a linear factor in (24) it is expected that this holds for any perturbation $f(\theta_0)$.

A further conclusion can be drawn from the local map equation (25). Below the threshold of complete stochasticity the Poincaré plot of the map consists of a mixture of undestroyed *KAM*-surfaces, islands and stochastic regions. As it has been discussed by MacKay [11] the *KAM*-surfaces with a noble or golden rotational transform are the most robust against destruction if the control parameter increases. Noble values of $t(\bar{\psi})$ are those numbers with a continued fraction representation ending on $[\ldots 1, 1, 1, 1, \ldots]$. Since the low shear system covers only a small regime on the y-axis, it is possible to

center this around a noble number of $t(\bar{\psi})$, which can be done by an appropriate choice of t_0.

Let us consider again a perturbation with a finite number of Fourier harmonics. Then there exists a finite number of resonant surfaces with primary islands. Starting with two arbitrary adjacent rational values of $t: t = m/l$ and $t = m'/l'$ the Farey tree of all rational number in between can be constructed by the repetitive procedure

$$\frac{m}{l}, \frac{m'}{l'} \rightarrow \frac{m+m'}{l+l'}. \tag{26}$$

On these corresponding rational surfaces secondary or higher order islands arise. Between m/l and m'/l' two noble numbers can be constructed with

$$t_1 = \frac{m + m'\sigma}{l + l'\sigma},$$

$$t_2 = \frac{m' + m\sigma}{l' + l\sigma}, \tag{27}$$

$\sigma = 1/2\,(\sqrt{5} - 1)$ is the golden mean. Of course, any two members of the Farey tree can be taken as a basis for noble irrationals, they are dense in any given domain. It is suggested that the two noble irrational given in (27) are the last ones to be destroyed in the given t-regime. In case of the standard map these two numbers are $t = 0.38196\ldots$ and $t = \sigma = 0.618033\ldots$ As Greene [3] has shown the *KAM*-surface of the standard map with $t = \sigma$ is the last one to be destroyed by a growing perturbation.

In application to a low shear stellarator we consider the intervall $0.4 \leqq t \leqq 0.5$ and a perturbation with 15 poloidal harmonics. The resonant surfaces are

$$t = \{2/5, 5/12, 3/7, 4/9, 5/11, 6/13, 7/15\}.$$

The size of the primary islands depends on the corresponding amplitudes $\varepsilon_{l,m}$ or on the Fourier harmonics in $f(\theta_0)$. We expect the smallest primary island to occur at $t = 7/15 = 0.4666\ldots$. Between this number and $t = 1/2$ the two noble irrationals $t = 0.469204\ldots$ and $t = 0.4725\ldots$ exist. Now, if the t-profile of the low shear stellarator is chosen appropriately with $t = 0.47$ in the center and $t = 0.48$ at the edge, all primary islands can be avoided and one of the most stable surfaces is included. If the perturbation spectrum contains higher harmonics than 15, this stable regime approaches $t = 1/2$ more closely. A similar situation occurs above $t = 1/2$ and in the neighbourhood of $t = 1/3$ and multiples of $1/2$.

IV. Numerical Results

Wendelstein VII-A is a low shear stellarator with the rotational transform varying only by 1% across the plasma radius. As a model of the rotational transform a function of the flux $t(\psi) = t_0 + t_1\psi$ was chosen with $t_1 = 0.01$. The perturbation is modelled by $h = 0$ and a Fourier series $g(\theta_0)$

$$g(\theta_0) = \sum_{l=1}^{15} \frac{K_l}{l} \sin l\theta_0 \tag{28}$$

with constants K_l given explicitly or following an exponential decay $K_l = K \exp(-\gamma l)$. In this latter case the δ-like perturbation is characterized by the two parameters K and γ. These parameters are chosen such that the map yields roughly the same island pattern as found from the field line tracing taking into account the current leads to the helix [2]. The numbers are $K = 4 \times 10^{-3}$ and $\gamma = 0.2$. In Fig. 4 the islands arising at $t = 1/2$, $\psi = 1$ are shown. The Cartesian coordinates of the plot are related to ψ, θ

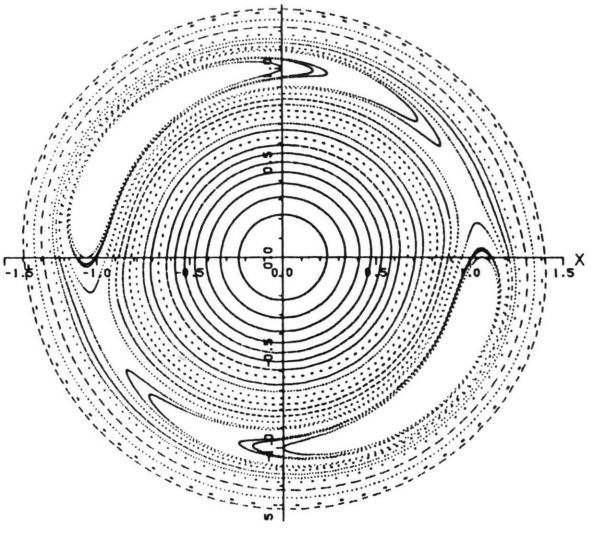

Fig. 4. Result of the mapping procedure following equation (17). $t_0 = 0.49$, $t_1 = 0.01$, $K = 4 \cdot 10^{-3}$, $\gamma = 0.2$. The resonant surface is at $t = 1/2$.

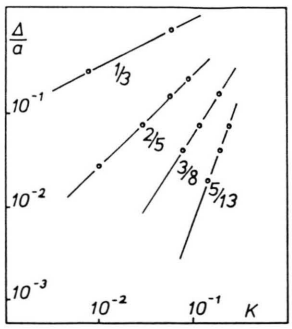

Fig. 5. Relative width of islands. $t_1 = 0.01$, $K_2 = K_3 = K$. The plot shows the growth of islands with the control parameter K.

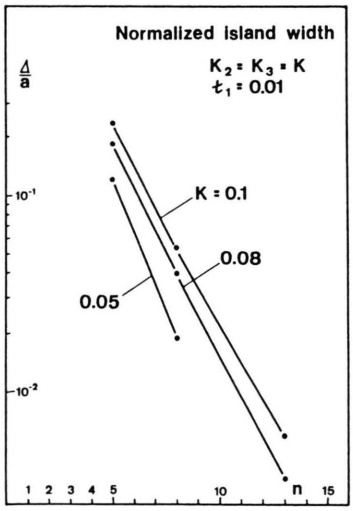

Fig. 6. Relative island width vs the period n. $t_1 = 0.01$, $K = K_2 = K_3$.

by $x = \sqrt{\psi}\cos\theta$, $y = \sqrt{\psi}\sin\theta$. Similar islands occur at $t = 1/3,\ 2/3, \ldots, m/n$. The size of the islands increases wih the perturbation parameter K and decreases with the period n which is the number of toroidal transits before the field line closes upon itself. Since the Fourier spectrum of the perturbation contains harmonics up to $l = 15$, the first generation of islands is created at all rational surfaces with denominator $n = 1, \ldots, 15$. The size of these islands increases with the square root of the control parameter K. The first generation of islands at two rational surfaces $t = m_1/n_1$ and $t = m_2/n_2$ gives rise to a second generation of islands at $t = (m_1 + m_2)/(n_1 + n_2)$. Continuing this process yields a sequence of rational surfaces with $t_k = m_k/n_k$, where the numerator and the denominator follow a Fibonacci series. The scaling of these islands was studied in the case of two first-generation islands with K_2 and K_3, higher Fourier harmonics being set to zero. As seen from Fig. 5, the first-generation island at $t = 1/3$ increases roughly as $\sqrt{K}$ ($K = K_2 = K_3$). The second-generation island at $t = 2/5$ already shows a faster increase and the third ($t = 3/8$) and fourth-generation islands ($t = 5/13$) increase with a higher power than the preceding generation. At a fixed control parameter the size of the island decays exponentially with the period n (Figure 6). The behavior at the chaos border, when *KAM* surfaces are destroyed, is determined by the high-n islands, whereas in the subcritical case only a finite number of low-generation islands, whose width is larger than the gyroradius of electrons, affect the plasma confinement.

The general trend of islands to decrease with n may explain the dependence of confinement on t_0 in Wendelstein VII-A. The biggest islands created by external perturbations arise at $t = 1/2$ and $t = 1/3$. The neighbourhood of these rational surfaces, however, contains rational surfaces with a high period n only. Islands on these surfaces are exponentially small. In Figs. 7–10 comparison is made with a fixed perturbation spectrum in different t-regimes. In Fig. 7 the region from $t = 0.45$ on the magnetic axis to $t = 0.47$ at the boundary is shown. The perturbation spectrum is given by

$$K_l = 6 \times 10^{-3} \exp(-0.05\, l)\,, \quad l = 1, \ldots, 15\,.$$

Islands can be seen at $t = 5/11$, $6/13$, $7/15$. In the adjacent regime $t = 0.47 - 0.49$, which lies closer to $t = 1/2$, the same perturbation does not generate visible islands (Figure 8). The Figs. 9 and 10 show the t-regime $0.44 - 0.46$ and $t = 0.43 - 0.45$. Similar behaviour is found slightly above $t = 1/2$ and in the neighbourhood of $t = 1/3$.

A magnification of the pictures shows smaller and smaller islands, which can be seen from Figs. 11–14 where the regions $1.1 \leqq x \leqq 1.5$ and $-0.2 \leqq y \leqq +0.2$ are shown. The small islands arise at $t = m_1 + m_2/n_1 + n_2$. For example, in Fig. 11 ($t = 0.45 - 0.46$) the two big islands occur at $t = 5/11$ and $t = 5/13$. These islands are created by the external perturbation,

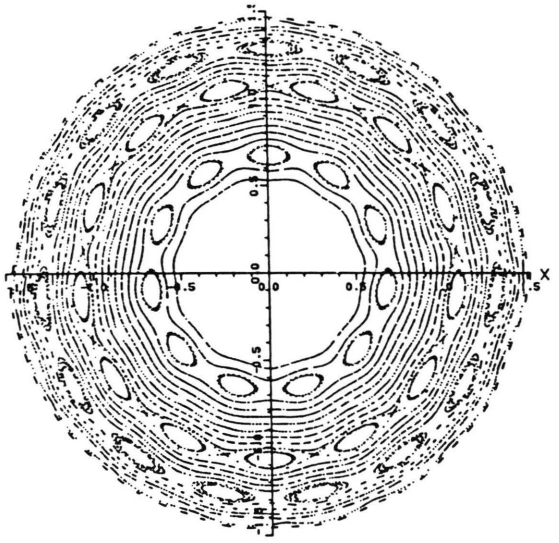

Fig. 7. Perturbed magnetic surfaces with $K = 6 \cdot 10^{-3}$, $\gamma = 0.05$. The regime of t is 0.45–0.47. $t_1 = 0.01$.

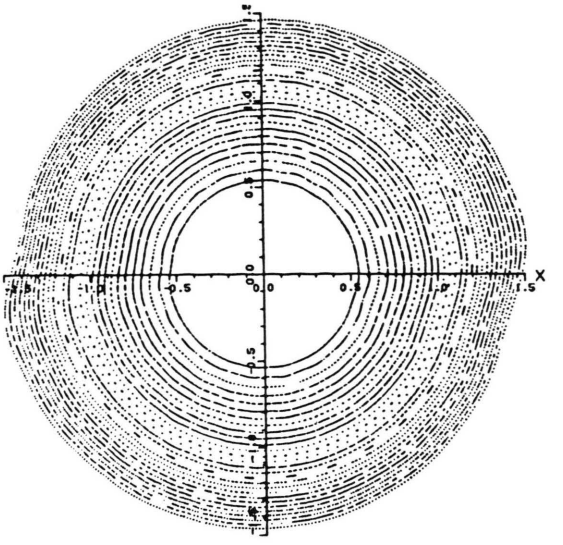

Fig. 8. Parameters as in Fig. 7. $t = 0.47-0.49$.

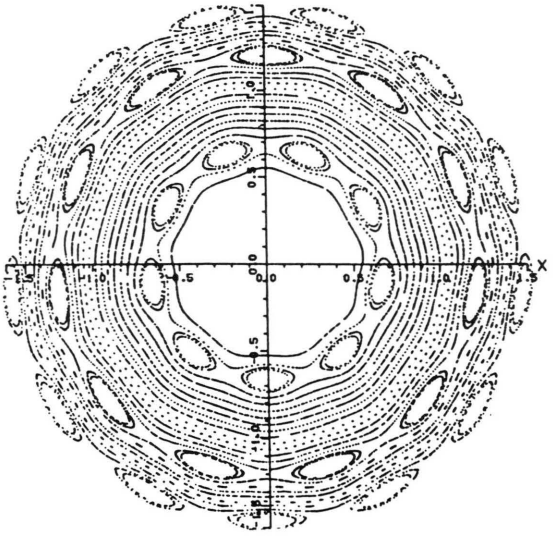

Fig. 9. $t = 0.44-0.46$, $K = 6 \cdot 10^{-3}$, $\gamma = 0.05$.

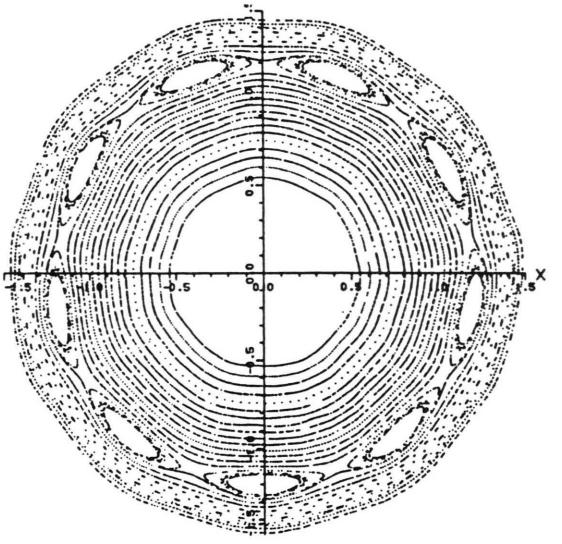

Fig. 10. $t = 0.43-0.45$, $K = 6 \cdot 10^{-3}$, $\gamma = 0.05$.

which contains 15 harmonics. The other smaller islands can be identified at $t = 11/24$, 16/36, 17/37, 21/46. An increase of the perturbation amplitude leads to a rapid increase of these high-generation islands and finally to stochasticity. As has been shown by MacKay [10], all area-preserving maps locally approach a universal map with an increase of the control parameter K. This means that the general pattern of island formation and transition to stochasticity becomes independent of the details

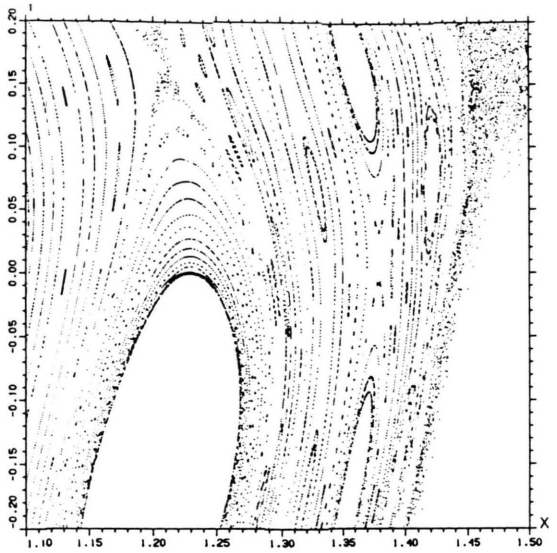

Fig. 11. Magnified area from the perturbed magnetic surface. $K = 8 \cdot 10^{-3}$, $\gamma = 0.05$, $t = 0.45-0.46$.

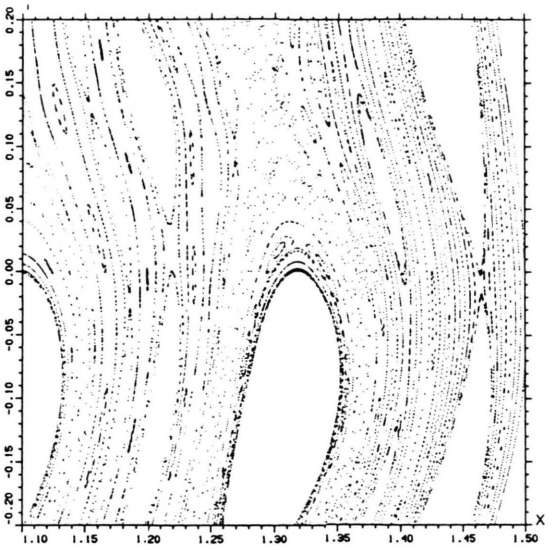

Fig. 13. $t = 0.46-0.47$.

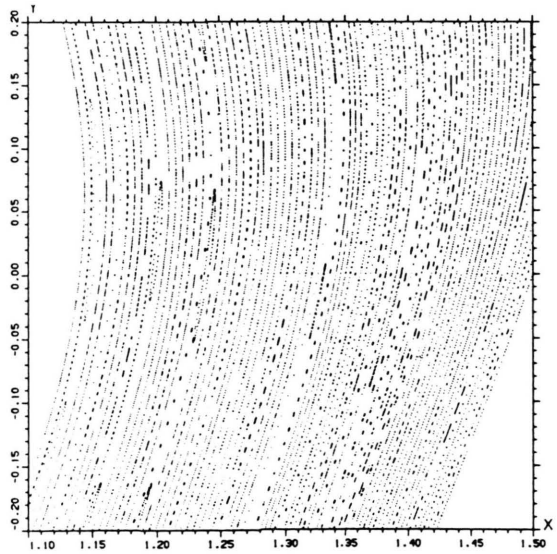

Fig. 12. Magnified area with $t = 0.48-0.49$. Parameters as in Figure 11.

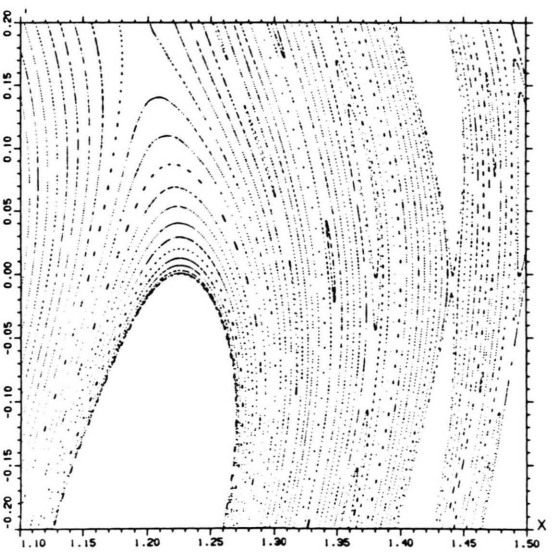

Fig. 14. $t = 0.44-0.45$.

of the specific map. Consequently the general results found for the map chosen above holds for all perturbations $h(\psi, \theta)$ of the unperturbed twist map.

The effect of shear has been studied by varying the parameter t_1 in the t-profile. Although the size of the islands decreases with higher shear, the distance between two adjacent rational surfaces decreases faster and after approximate overlapping of the islands the region in between disintegrates into a stochastic sea. As can be seen from Fig. 15, the

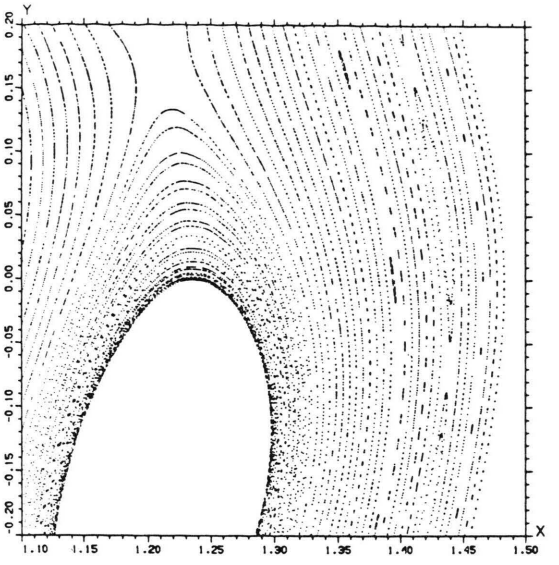

Fig. 15. Reduction of shear to $t_1 = 0.005$. The big island corresponds to $t_0 = 5/11$. $K = 8 \cdot 10^{-3}$, $\gamma = 0.05$.

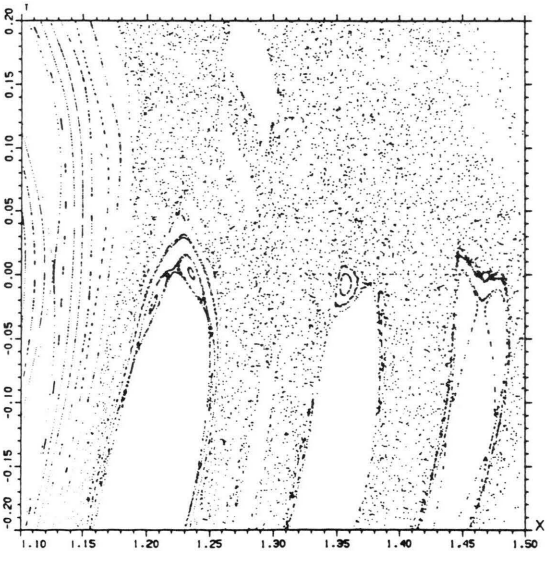

Fig. 16. Effect of doubling the shear. $t_1 = 0.02$, $K = 8 \cdot 10^{-3}$, $\gamma = 0.05$.

island at $t = 5/11$ grows if the shear is reduced by a factor of two. This figure has to be compared with Figure 11. An increase of the shear by a factor of two reduces the distance between the islands $t = 5/12$, 6/13, 7/15 and the region in between becomes stochastic (Figure 16).

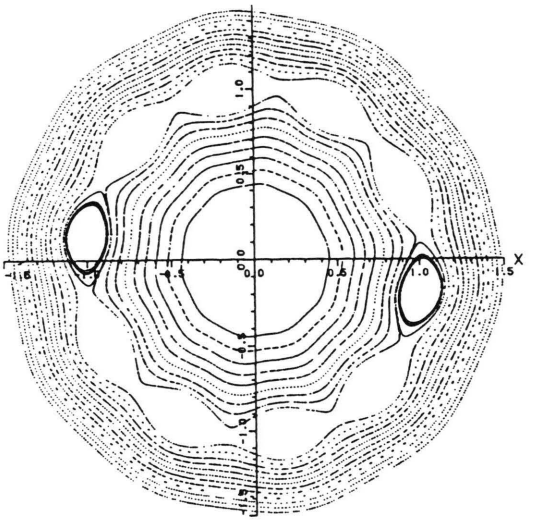

Fig. 17. Localized perturbation in every field period, $t = 0.49 - 0.51$, $K = 4 \cdot 10^{-3}$, $\gamma = 0.2$. The arrangement of the perturbation preserves the five-fold symmetry.

Multimap:

$\alpha_1 = 20.000$	$\beta_1 = 0.200$	$\gamma_1 = 0.200$	$K_1 = 0.020$	$\iota_0 = 0.490$
$\alpha_2 = 20.000$	$\beta_2 = 0.200$	$\gamma_2 = 0.200$	$K_2 = 0.020$	$\iota_1 = 0.010$
$\alpha_3 = 20.000$	$\beta_3 = 0.200$	$\gamma_3 = 0.200$	$K_3 = 0.020$	$\iota_2 = 0.000$
$\alpha_4 = 20.000$	$\beta_4 = 0.200$	$\gamma_4 = 0.200$	$K_4 = 0.020$	
$\alpha_5 = 20.000$	$\beta_5 = 0.200$	$\gamma_5 = 0.200$	$K_5 = 0.020$	

In the preceding analysis the perturbation is localized to an angle ψ_s in the toroidal direction. Thus the perturbation breaks the symmetry of the stellarator field which is five fold in the case of W VII-A. If the same perturbation occurred in each period, its effect on island formation would be much smaller. In order to study this behaviour, the mapping process described in (3) was applied to each field period. For this purpose the toroidal angle of the perturbation and its poloidal localization have to be specified for each period. By proper choosing all parameters characterizing the perturbation in each field period we can either preserve the symmetry or break the symmetry. In Fig. 17 it is shown how the same perturbation which creates two islands at $t = 1/2$ (see Fig. 4) leads to 10 small islands if it occurs in each field period. The amplitude K is 0.02, which is five times as high as in Figure 4. If the parameters are chosen in such a way that the position of the perturbation is different in each field period, the symmetry of the system is broken and large islands appear again. This is

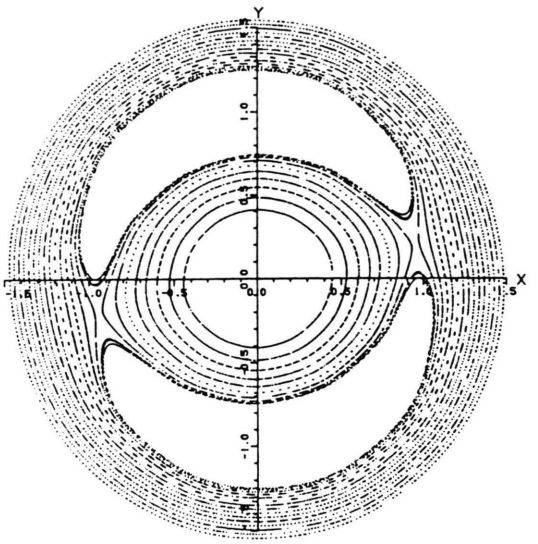

Fig. 18. The perturbation is identical in every field period, except for the poloidal locations. The five-fold symmetry is destroyed.

Multimap:

$\alpha_1 = 0.000$	$\beta_1 = 0.200$	$\gamma_1 = 0.200$	$K_1 = 0.004$	$\iota_0 = 0.490$
$\alpha_2 = -35.000$	$\beta_2 = 0.200$	$\gamma_2 = 0.200$	$K_2 = 0.004$	$\iota_1 = 0.010$
$\alpha_3 = -70.000$	$\beta_3 = 0.200$	$\gamma_3 = 0.200$	$K_3 = 0.004$	$\iota_2 = 0.000$
$\alpha_4 = -105.000$	$\beta_4 = 0.200$	$\gamma_4 = 0.200$	$K_4 = 0.004$	
$\alpha_5 = -140.000$	$\beta_5 = 0.200$	$\gamma_5 = 0.200$	$K_5 = 0.004$	

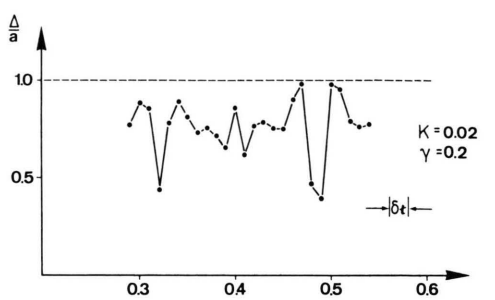

Fig. 19. Effective plasma radius Δ/a vs external rotational transform ι_0.

shown in Fig. 18 where the amplitude of the perturbation is the same as in Fig. 4 ($K = 0.004$). A similar situation holds for every rational magnetic surface and it can be shown from the Hamiltonian form of the field line equations (6) that a perturbation equally distributed in every field period is much less destructive than one occurring only once around the torus.

In estimating the effect of islands on plasma confinement the size of the islands may be a good figure of merit for the reduction of the effective plasma radius. For this purpose the size of the islands was calculated from the residues of the map at the fixed points. For an island at $t = m/n$ the fixed point was found by minimizing the distance between a point P and its image $T^n(P)$. The linearization of the map T^n around a fixed point, the so-called tangent map DT yields the Jacobian M at the fixed points and from this the excentricity of the ellipses at the o-points and the angle between separatrices at the x-points can be calculated [3]. These quantities are used to estimate the radial width $\delta\psi$ of the island. The radial width of the island can only be defined approximately, since in general separatrix consists of a stochastic region. The sum of all islands $\sum \delta\psi$ with $\delta\psi \geqq 10^{-3}$ was calculated and normalized to the maximum value a of ψ. Figure 19 shows the effective plasma cross section $\Delta = \sum \delta\psi - a$ vs t for a fixed external perturbation with $K = 0.02$ and $\gamma = 0.2$, $\delta_t = 0.02$. It can be seen that the effective plasma cross section defined by the area not covered by islands roughly follows the same pattern as the experimentally found confinement time or plasma energy.

V. Conclusions

Like the problem of a kicked pendulum the effect of toroidally localized perturbations on unperturbed magnetic surfaces can be studied with a discrete map of the poloidal plane onto itself. The results show that the influence of a fixed perturbation on island formation differs according to the region of rotational transform and shear. The regions close to low-order rational surfaces $t = 1/2$ and $t = 1/3$ are less destroyed by islands than others. This might give an explanation of the good confinement observed in these regions. Two effects of islands have to be expected: one is the modification of the equilibrium and the other one the enhanced plasma diffusion. Plasma equilibrium in the presence of islands is still an unsolved problem, neither a successful analytic theory nor a numerical code having been established to deal with this problem. The presence of electric fields which follow the pattern of the islands may lead to convective cells and result in enhanced plasma losses. Also neo-

classical diffusion processes should be enhanced by islands since particles can jump from island to island by Coulomb collisions. Monte Carlo simulation by White et al. [12] have verified this effect. Although these are only qualitative considerations, they make plausible why the region with high-order rational magnetic surfaces exhibits better confinement than those with lower ones.

There seems to be an optimum value of the shear parameter t_1. If the shear is too small, any island can grow to an intolerable size. If the shear is too large, island overlapping leads to rapid destruction of the magnetic surfaces. In the W VII-A stellarator the shear is modified by the plasma pressure and by the pressure driven currents. In order to understand the details of the experimental results, these modifications have to be taken into account.

In principle symmetry-breaking perturbation can be avoided in stellarators. In a modular stellarator all systematic perturbations like current leads and joints can be made equal in every field period, what is left being statistical errors coming from the construction and the assembly. Internal modifications of the field due to the finite plasma pressure preserve the symmetry, and thus they should be less effective.

Acknowledgements

The author would like to thank I. Ott for preparing the *MAP* code for her assistance with the numerical calculations.

[1] H. Renner, W VII-A Team, NI Group, Pellet Injection Group, Proc. 10th Conf. on Plasma Physics and Contr. Nuclear Fus. Res. London 1985, IAEA, Vienna, CN-44/D-I-1.
[2] S. Rehker and H. Wobig, Report IPP 2/218, 1974.
[3] J. M. Greene, J. Math. Phys. **20,** 1183 (1973).
[4] J. M. Greene: in "Nonlinear Dynamics" (R. G. H. Helleman ed.), Academy of Sciences, New York 1980, p. 80.
[5] B. V. Chirikov, Phys. Rep. **52,** 265 (1979).
[6] J. Moser, "Nonlinear Problems", ed. R. E. Langer, University of Madison Press, Madison, Wisconsin 1963, p. 139.
[7] J. R. Cary and R. G. Littlejohn, Ann. Phys. **151,** 1 (1983).
[8] A. Salat: Z. Naturforsch. **40 a,** 959 (1985).
[9] M. P. Bernardin and J. A. Tataronis, J. Math. Phys. **26,** Sept. 1985 (9).
[10] K. Elsässer, Plasma Phys. **28** (1986).
[11] R. S. MacKay, Physica 7D, **1983,** p. 283.
[12] R. B. White, A. H. Boozer, R. Goldston, R. Hay, J. Albert, and C. F. F. Karney, Proc. 9th Conf. on Plasma Physics and Contr. Nuclear Fus. Res., Baltimore 1982, IAEA, Vienna 1983, Vol. III, p. 391.